frontiers | Frontiers in Materials

ORIGINAL RESEARCH
published: 19 May 2022
doi: 10.3389/fmats.2022.913326

Flexible $La_{0.67}Sr_{0.33}MnO_3$:ZnO Nanocomposite Thin Films Integrated on Mica

Xiong Zhang[1,2,3,4], *Hui Yang*[2,3,4], *Guoliang Wang*[1,2,3,4], *Yi Zhang*[2,3,4] *and Jijie Huang*[1,2,3,4]*

[1]School of Materials, Shenzhen Campus of Sun Yat-sen University, Shenzhen, China, [2]Guangdong Key Laboratory of Magnetoelectric Physics and Devices, School of Materials, Sun Yat-sen University, Guangzhou, China, [3]State Key Laboratory of Optoelectronic Materials and Technologies, School of Physics, Sun Yat-sen University, Guangzhou, China, [4]Centre for Physical Mechanics and Biophysics, School of Physics, Sun Yat-sen University, Guangzhou, China

The integration of functional oxide thin films on flexible substrates is critical for their application in flexible electronics. Here, to achieve flexible perovskite manganite oxide film with excellent low-field magnetoresistance (LFMR) effect, textured $La_{0.67}Sr_{0.33}MnO_3$ (LSMO):ZnO nanocomposite film was deposited on a flexible mica substrate with ZnO buffer using pulsed laser deposition (PLD). Compared to the polycrystalline LSMO:ZnO nanocomposite film directly deposited on mica without buffer, the LSMO:ZnO/ZnO/mica sample exhibits larger saturation magnetization (164 emu/cm^3) and higher Curie temperature (~319 K), which results from the crystallinity and strain in the LSMO phase. In addition, the LSMO:ZnO/ZnO/mica film presents a high MR value of ~39% at 10 K under 1 T. Furthermore, the good mechanical stretchability and property stability of the nanocomposite thin films have been demonstrated with mechanical bending.

Keywords: flexible mica, nanocomposite thin film, magnetoresistance, pulsed laser deposition, manganite oxide

OPEN ACCESS

Edited by:
Adeel Afzal,
University of the Punjab, Pakistan

Reviewed by:
Stefan Irimiciuc,
National Institute for Laser Plasma and Radiation Physics, Romania
Amir Habib,
University of Hafr Al Batin, Saudi Arabia
Weishi Tan,
Hunan City University, China

***Correspondence:**
Jijie Huang
huangjj83@mail.sysu.edu.cn

Specialty section:
This article was submitted to Thin Solid Films, a section of the journal Frontiers in Materials

Received: *05 April 2022*
Accepted: *20 April 2022*
Published: *19 May 2022*

Citation:
Zhang X, Yang H, Wang G, Zhang Y and Huang J (2022) Flexible $La_{0.67}Sr_{0.33}MnO_3$:ZnO Nanocomposite Thin Films Integrated on Mica. Front. Mater. 9:913326. doi: 10.3389/fmats.2022.913326

INTRODUCTION

Owing to the novel physical properties and potential applications in advanced electronic and spintronic devices, perovskite manganite with the generic formula of $RE_{1-x}AE_xMnO_3$ (RE = rare earth, AE = Ca, Sr, Ba, and Pb) has attracted intensive research interests (Wang et al., 2014; Zheng et al., 2019).The strong coupling of spin, charge, orbital, and lattice degrees of freedom results in exotic magnetic and transport properties in perovskite manganite (Zhang et al., 2022; Moshnyaga et al., 2003). For example, colossal magnetoresistance (CMR) has been achieved in doped perovskite manganite, despite the fact that a high magnetic field (several Tesla) is required, which limits its further application (Kang et al., 2012; Wang et al., 2016). Therefore, extensive research efforts have been devoted to exploring magnetoresistance (MR) under low field, termed low-field magnetoresistance (LFMR). The LFMR effect results from spin-polarized tunneling, and spin-dependent scattering occurs at grain/phase boundaries (Hwang et al., 1996; Wu et al., 2018), which is different from the double exchange mechanism, magnetopolaron mechanism, and Jahn–Teller effect for CMR (Tokura and Tomioka, 1999; Liu et al., 2013). Various approaches have been employed to improve the LFMR value in manganites, such as introducing artificial grain boundaries, magnetic domain walls, and secondary phases (Ning et al., 2014; Wu et al., 2018).

Incorporating an insulating secondary phase in both composite bulk and thin film has been widely adopted as an effective approach to improve the LFMR effect (Yao et al., 2003; Navin and Kurchania, 2018). Till date, various composite materials involving manganites and insulating secondary phases have been reported to effectively enhance the LFMR effect, such as LSMO:NiO (Ning et al., 2015;

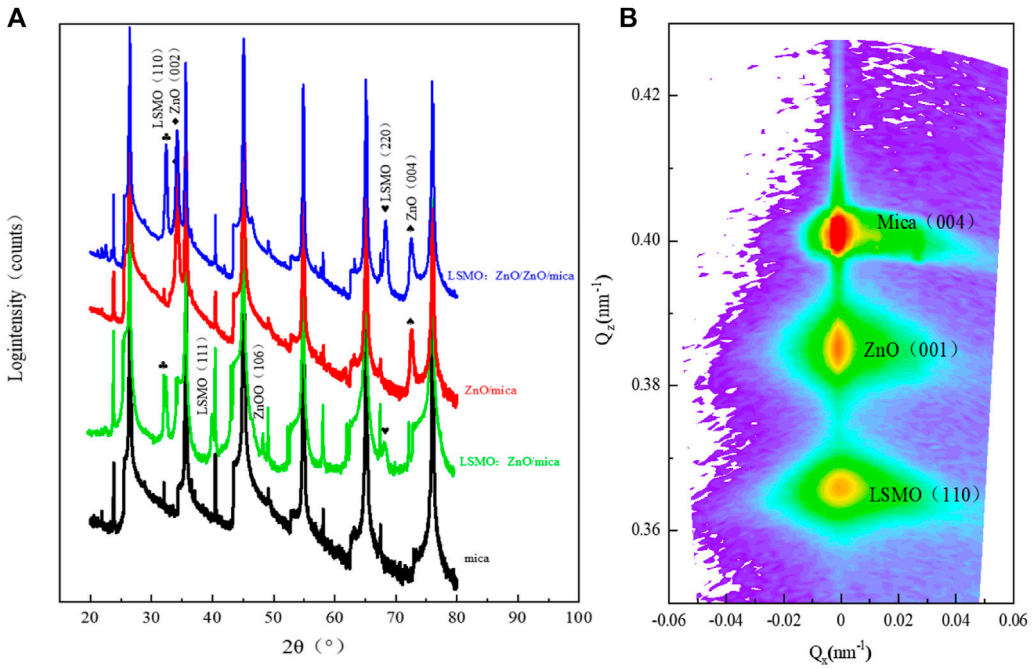

FIGURE 1 | (A) X-ray diffraction (XRD) θ-2θ pattern of the mica, LSMO:ZnO/mica, ZnO/mica, and LSMO:ZnO/ZnO/mica samples. **(B)** Reciprocal space map (RSM) of the LSMO:ZnO/ZnO/mica sample.

Zhang et al., 2020), LSMO:MgO (Chen et al., 2016), and LSMO:Mn_3O_4 (Bi et al., 2011). For example, a vast enhancement of the LFMR value of ~34.3% has been achieved in $(La_{0.7}Sr_{0.3}MnO_3)_{0.5}$:$(CeO_2)_{0.5}$ composite film under 1 T at 45 K (Fan et al., 2015). Recently, 3D nanocomposite thin films have also been developed to further improve the LFMR value *via* 3D strain engineering (Sun et al., 2018; Sun et al., 2019).

However, most of the nanocomposite thin films with the enhanced LFMR effect have been deposited on rigid substrates (Si, $SrTiO_3$, Al_2O_3, etc.) (Tiwari et al., 2003; Valencia et al., 2003; Zhang et al., 2013; Liao and Zhang, 2019; Carrero et al., 2020), which is not applicable for flexible device integration. Due to the contradiction of the low melting point of flexible organic substrates and the high-temperature process for high-quality oxide thin film deposition, it is challenging to achieve high-quality flexible nanocomposite thin films. Recently, fluorophlogopite mica (F-mica) has been considered as an ideal flexible substrate for the high-temperature process because of its high melting point (1,300°C), cleavable layered structure, and ultrasmooth surface (Liu and Wang, 2020). Various complex oxide thin films have been demonstrated on mica with high film quality, such as $La_{0.7}Sr_{0.3}MnO_3$, $Pr_{0.5}Ca_{0.5}MnO_3$, and $BiFeO_3$ (Fan et al., 2019; Zhang et al., 2019; Ma et al., 2020; Yen et al., 2020; Hou et al., 2021), as well as several nanocomposite thin films of $La_{0.67}Sr_{0.33}MnO_3$:NiO (Huang et al., 2020), $BaTiO_3$:Cu (Liu et al., 2020), and $BiFeO_3$:$CoFe_2O_4$ (Amrillah et al., 2017).

To realize the LFMR effect of nanocomposite thin films on flexible substrates, in this study, $La_{0.67}Sr_{0.33}MnO_3$ (LSMO):ZnO nanocomposite films have been grown on mica substrates using the pulsed laser deposition (PLD) technique as this is the most used method for depositing nanocomposite thin films. The films were deposited on mica with or without a ZnO buffer layer, to achieve textured and polycrystal quality, respectively. Then the magnetic and magnetoresistance properties of the films have been explored, and the bending stability has been tested. This work paves a route toward the application of LFMR in nanocomposite thin films for flexible electronic and spintronics.

RESULTS AND DISCUSSION

Standard θ-2θ X-ray diffraction (XRD) was first characterized for the samples, as shown in **Figure 1A**; the black, green, red, and blue curves present the patterns of mica, LSMO:ZnO/mica, ZnO/mica, and LSMO:ZnO/ZnO/mica, respectively. For the LSMO:ZnO/mica sample, LSMO (110), (220), and (111) diffraction peaks were identified, which indicates the polycrystalline nature of this sample. In order to achieve the out-of-plane preferred growth of LSMO:ZnO composite films on mica, a ZnO buffer layer was introduced, as ZnO can grow epitaxially on mica (red curve). For the LSMO:ZnO/ZnO/mica sample, only LSMO (*ll*0) and ZnO (00*L*) peaks were observed, which indicates the textured growth of the nanocomposite film (blue curve). Then, the d-spacing values of LSMO and ZnO can be calculated based on Bragg's equation, for example, $d_{LSMO(110)}$ = 2.76Å, $d_{ZnO(002)}$ = 2.62Å, which induces a tensile strain of 0.495% in LSMO along the (110) direction and a compressive strain of –0.769% in ZnO along the (001) direction. The strain is mainly caused by the lattice mismatch between LSMO and ZnO along the

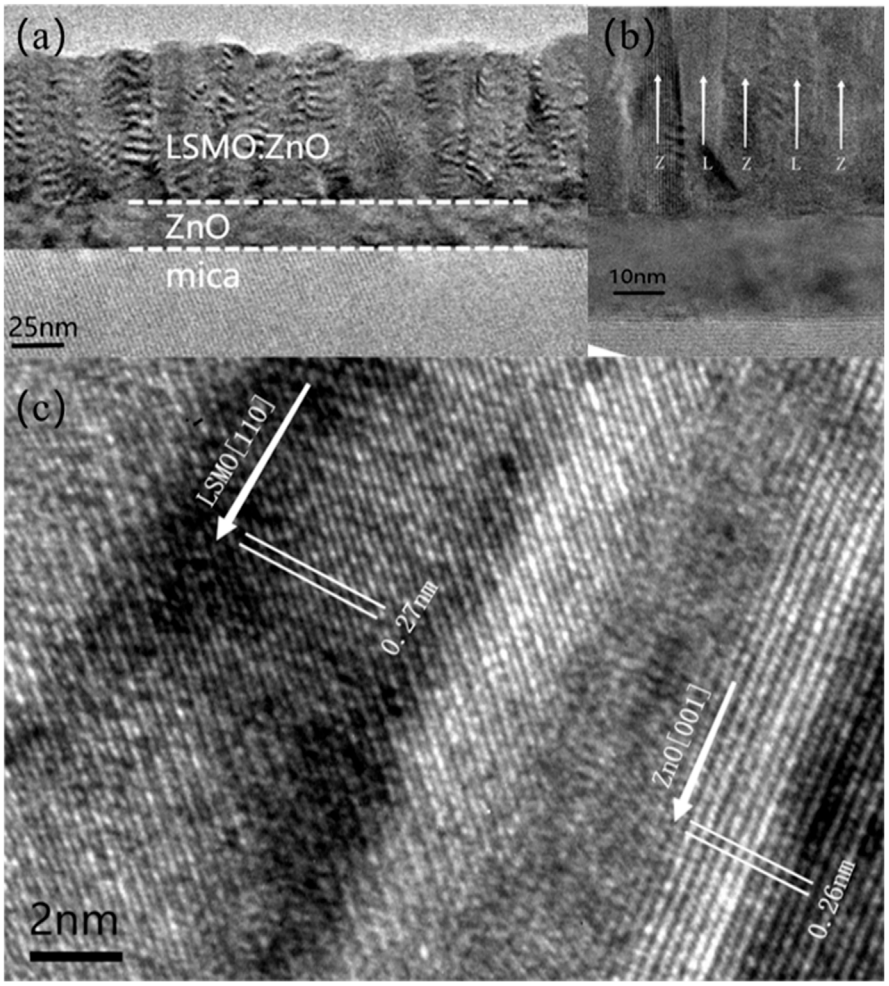

FIGURE 2 | Microstructure characterization on the LSMO:ZnO thin film on buffered mica substrates. **(A)** Low-magnification, **(B)** medium-magnification, and **(C)** high-resolution TEM images of LSMO:ZnO on the ZnO buffered mica substrate.

vertical interface, which could affect the physical properties of the nanocomposite thin film. The reciprocal space map (RSM) of the LSMO:ZnO/ZnO/mica sample in **Figure 1B** further confirms the textured growth of both LSMO and ZnO phases in the nanocomposite film.

Then, to explore the microstructure of the LSMO:ZnO/ZnO/mica sample, transmission electron microscopy (TEM) characterization has been carried out. **Figure 2A** presents a low-magnification cross-sectional TEM image, and the thickness of the ZnO buffer layer and the LSMO:ZnO composite layer can be estimated to be ~20 and ~70 nm, respectively. The LSMO:ZnO film exhibits a typical vertically aligned nanocomposite (VAN) structure with ZnO nanopillars embedded in the LSMO matrix, as marked by the white arrows in **Figure 2B**, which also shows a clear and sharp LSMO/ZnO interface with limited inter-diffusion. **Figure 2C** shows a high-resolution TEM (HRTEM) image of the LSMO phase and ZnO phase, which reveals out-of-plane preferred growth of the LSMO and ZnO on ZnO buffered mica substrate. The out-of-plane d-spacing of the LSMO phase and the ZnO phase can be determined to be 0.27 nm and 0.26 nm, respectively, which is inconsistent with the XRD results.

In addition, physical properties of the nanocomposite thin films on mica were investigated, and the robustness of the properties with the bending process was explored. Mica substrate was first cleaved into a thin layer form in order to gain enhanced flexibility, and then the flexible LSMO:ZnO nanocomposite films were made to endure various bending cycles with a radius of 10 mm, as shown in the inset of **Figure 3A**. **Figure 3A** shows the M-H curves measured at 10 K of the LSMO:ZnO thin films with the applied magnetic field perpendicular (OP: out-of-plane) to the film surface. As is seen, the textured film exhibits larger saturation magnetization (~164 emu/cm^3) than its polycrystalline counterpart (~131 emu/cm^3), which is caused by the different strain state in LSMO for the two films, as well as the crystallinity and growth orientation of the films (Wang et al., 2017). In the polycrystal sample, tension strains of 0.75% and 0.826% were induced in the LSMO (110) and LSMO (111) phases, both larger than 0.495% in the LSMO (110) phase of

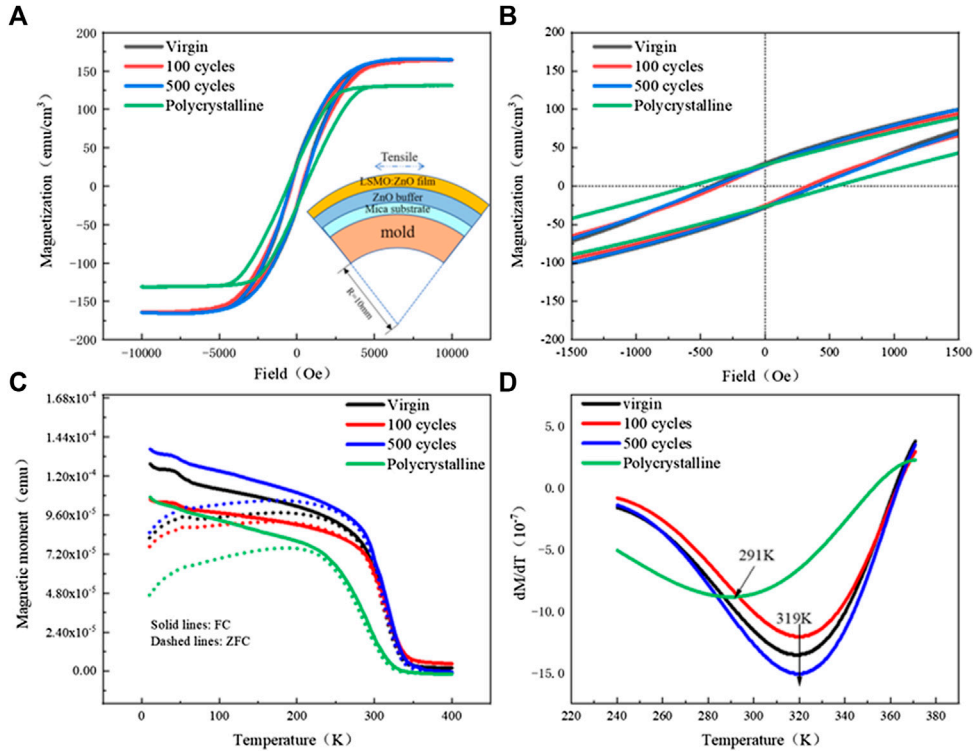

FIGURE 3 | Magnetic properties of the LSMO:ZnO thin films on mica. **(A)** M-H curves measured at 10 K and **(B)** enlarged area to show the coercivity; **(C)** FC and ZFC M-T curves and **(D)** dM/dT versus temperature under a 1T field.

the textured sample. The stronger tensile strain may increase the volume fraction of the antiferromagnetic phase that makes little contribution to the magnetization, which decreases the ferromagnetic order and reduces the saturation magnetization (Shen et al., 2012). We also measured the M-H curves of the LSMO:ZnO/ZnO/mica sample with 100 and 500 bending cycles and no apparent change was observed, which indicates the robustness of the film with the bending process. **Figure 3B** is the enlarged area to show the coercivity of the samples (H_C, ~349 Oe), which is comparable to the reported values (Haque et al., 2019). It is also noted that the polycrystal LSMO:ZnO exhibits slight higher coercivity, which indicates that the increase in lattice distortion in polycrystal LSMO:ZnO film causes stronger pinning centers for the magnetic domains, thus leading to an enhancement in the coercivity (Gu et al., 2012; Yin et al., 2017).

Figure 3C compares the temperature-dependent magnetization (M-T, 5–400 K) curves under 1,000 Oe field-cooling (FC) and zero-field cooling (ZFC) of the LSMO:ZnO nanocomposite thin films. The magnetization monotonically decreases with increasing temperature under FC, while under ZFC, it increases gradually to a maximum value (blocking temperature: T_B) before decreasing monotonically as temperature increases. Furthermore, a bifurcation between the ZFC and FC curves has been observed at an irreversibility temperature (T_{irr}), which is slightly higher than T_B. Such bifurcation might be caused by the existence of the spin glass state and/or the non-uniformity of the magnetic phase (Wang et al., 2021; Wang et al., 2015). Then, the Curie temperature (T_c) could be determined by the M-T curves where magnetization starts to increase dramatically, which is also the magnetic phase transition temperature. Here, T_c can be determined to be ~315 K and ~291 K for the textured and polycrystalline LSMO:ZnO composite films, respectively, derived from the peak in the $\frac{dM}{dT} - T$ curves shown in **Figure 3D**. Such deviation of T_c can be interpreted using the Jahn–Teller distortion theory by considering a stain-induced distortion of the MnO_6 octahedra (Millis et al., 1998).

Last, the magnetoresistance (MR) property of the flexible LSMO:ZnO textured composite films has been investigated. The temperature-dependent resistivity (R-T) curves with a magnetic field of zero or 1 T are plotted in **Figure 4A**, which present the same trend for the bent samples as the virgin film. Based on the R-T data, MR values were derived using the equation of $MR = \frac{(R_0 - R_H)}{R_0} \times 100\%$ and plotted in **Figure 4B**. The MR value decreases with increasing temperature and minor difference was observed after the bending process, which indicates the strong durability of the textured LSMO:ZnO composite film on mica. The polycrystal sample presents slightly different MR values throughout the entire measured temperature, which might be a result of the different microstructures and strain states between the two samples. The maximum MR value of the samples is ~40% at low temperature, which is higher than those of the reported LSMO:ZnO composite films on rigid substrates, such as Si (~32%, 20 K) (Zhang et al., 2013), STO (31%, 154 K) (Chen et al., 2011), and Al_2O_3 (12%, 77 K) (Kang et al., 2006) under an applied field of 1 T. Overall, the LSMO:ZnO on mica presents strong MR effect compared to the

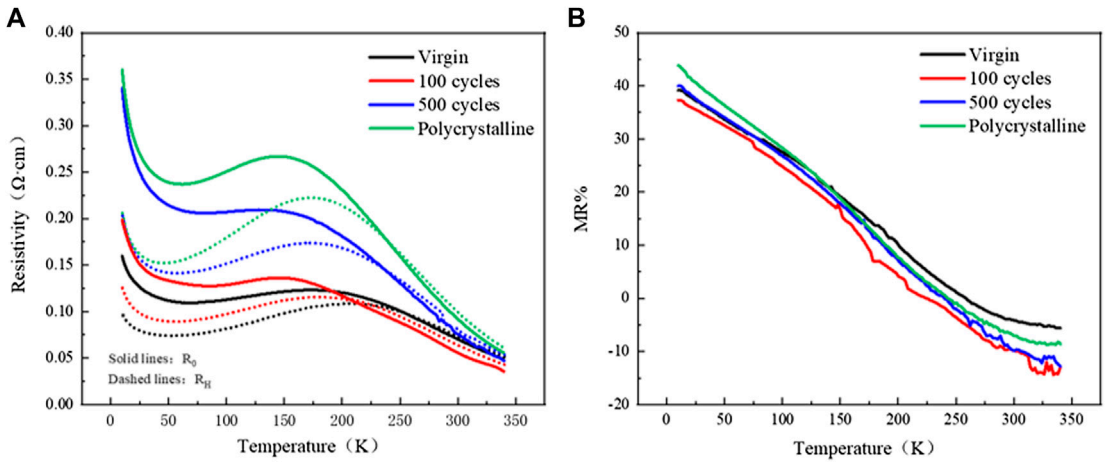

FIGURE 4 | (A) R-T curves (with a magnetic field of zero or 1 T) and **(B)** temperature dependence of MR for textured LSMO:ZnO films under different bending cycles (virgin, 100, and 500 times).

same films on other substrates, and the property is stable after bending, which indicates its promising potential for flexible device applications.

CONCLUSION

In summary, we have fabricated LSMO:ZnO nanocomposite thin films on mica substrates with or without ZnO buffer, which results in textured or polycrystal films. The nanocomposite films show excellent ferromagnetic and magnetoresistance properties. For example, strong magnetic response and high MR value of ~40% at 10 K have been achieved, and minor deterioration was observed after the bending process, which indicates the great mechanical stability of the flexible LSMO:ZnO nanocomposite thin films. Our study paves the way for an exciting new avenue to the next-generation flexible smart electronics or spintronics.

EXPERIMENT DETAILS

Target Preparation

The LSMO:ZnO composite target (molar ratio of 1:1) was prepared using a conventional solid-state sintering process. A stoichiometric mixture of La_2O_3, MnO_2, $SrCO_3$, and ZnO powders were grounded, pressed into a disk, and annealed at 1,200°C in air for 6 h. The commercial ZnO target was used to deposit the ZnO buffer layer.

Thin Film Growth

The ZnO buffer layer and LSMO-ZnO composite film were grown on F-mica substrate *via* a pulsed laser deposition (PLD) approach using a KrF excimer laser (λ = 248 nm). Before deposition, the chamber was pumped to a base pressure of 3.0×10^{-6} mbar or more. During deposition, the ZnO and LSMO-ZnO layers were deposited at 650°C, 6.66×10^{-2} mbar O_2 and 750°C, 2.66×10^{-2} mbar O_2, respectively. The laser fluence and repetition frequency were controlled at 0.65 mJ/cm^2 and 5 Hz, respectively, for all the depositions. After deposition, the samples were cooled down at a cooling rate of 10°C min^{-1} under an oxygen pressure of 266 mbar.

Characterizations

The crystal structure and microstructure of the films were conducted by X-ray diffraction (XRD) (Panalytical X'Pert X-ray diffractometer) and transmission electron microscopy (TEM) (FEI Tecnai F30). Temperature dependence of magnetization and magnetic hysteresis curves were measured using a SQUID magnetometer (MPMS: Quantum Design). Resistance in dependence of temperature (R-T) measurement was conducted using a physical property measurement system (PPMS: Quantum Design).

DATA AVAILABILITY STATEMENT

The original contributions presented in the study are included in the article/Supplementary Material; further inquiries can be directed to the corresponding author.

AUTHOR CONTRIBUTIONS

JH contributed to conception and design of the study. XZ grew the thin films and measured the physical properties. HY and YZ made the TEM sample and carried out the imaging. XZ wrote the first draft of the manuscript. All authors contributed to manuscript revision and read and approved the submitted version.

FUNDING

This work was supported by the Guangdong Basic and Applied Basic Research Foundation (2019A1515111029) and the Shenzhen Science and Technology Program (JCYJ20210324133610028).

REFERENCES

Amrillah, T., Bitla, Y., Shin, K., Yang, T., Hsieh, Y.-H., Chiou, Y.-Y., et al. (2017). Flexible multiferroic bulk heterojunction with giant magnetoelectric coupling via van der waals epitaxy. *ACS Nano* 11 (6), 6122–6130. doi:10.1021/acsnano.7b02102

Bi, Z., Weal, E., Luo, H., Chen, A., MacManus-Driscoll, J. L., Jia, Q., et al. (2011). Microstructural and Magnetic Properties of (La0.7Sr0.3MnO3)0.7: (Mn3O4) 0.3 Nanocomposite Thin Films. *J. Appl. Phys.* 109 (5), 054302. doi:10.1063/1.3552594

Carrero, A., Roman, A., Aguirre, M., and Steren, L. B. (2020). Nanoscale Structural Characterization of Manganite Thin Films Integrated to Silicon Correlated with Their Magnetic and Electric Properties. *Thin Solid Films* 709, 138189. doi:10.1016/j.tsf.2020.138189

Chen, A., Bi, Z., Tsai, C.-F., Lee, J., Su, Q., Zhang, X., et al. (2011). Tunable Low-Field Magnetoresistance in (La0.7Sr0.3MnO3)0.5: (ZnO)0.5 Self-Assembled Vertically Aligned Nanocomposite Thin Films. *Adv. Funct. Mat.* 21 (13), 2423–2429. doi:10.1002/adfm.201002746

Chen, A., Hu, J.-M., Lu, P., Yang, T., Zhang, W., Li, L., et al. (2016). Role of Scaffold Network in Controlling Strain and Functionalities of Nanocomposite Films. *Sci. Adv.* 2 (6), e1600245. doi:10.1126/sciadv.1600245

Fan, M., Zhang, W., Khatkhatay, F., Li, L., and Wang, H. (2015). Enhanced Tunable Magnetoresistance Properties over a Wide Temperature Range in Epitaxial (La0.7Sr0.3MnO3)1−x: (CeO2)x Nanocomposites. *J. Appl. Phys.* 118 (6), 065302. doi:10.1063/1.4928160

Fan, J., Xie, Y., Qian, F., Ji, Y., Hu, D., Tang, R., et al. (2019). Isotropic Magnetoresistance and Enhancement of Ferromagnetism through Repetitious Bending Moments in Flexible Perovskite Manganite Thin Film. *J. Alloys Compd.* 806, 753–760. doi:10.1016/j.jallcom.2019.07.207

Gu, M., Song, C., Yang, F., Arenholz, E., Browning, N. D., and Takamura, Y. (2012). Tuning Magnetic and Transport Properties through Strain Engineering in La0.7Sr0.3MnO3/La0.5Sr0.5TiO3 Superlattices. *J. Appl. Phys.* 111 (8), 084906. doi:10.1063/1.4705397

Haque, A., Mahbub, A. R., Abdullah-Al Mamun, M., Reaz, M., and Ghosh, K. (2019). Fabrication and Thickness-dependent Magnetic Studies of Tunable Multiferroic Heterostructures (CFO/LSMO/Lao). *Appl. Phys. A* 125 (5), 357. doi:10.1007/s00339-019-2620-y

Hou, W., Zhao, S., Wang, T., Yao, M., Su, W., Hu, Z., et al. (2021). Manipulation of Microwave Magnetism in Flexible La0.7Sr0.3MnO3 Film by Deformable Ionic Gel Gating. *Appl. Surf. Sci.* 563, 150074. doi:10.1016/j.apsusc.2021.150074

Huang, J., Wang, H., Wang, X., Gao, X., Liu, J., and Wang, H. (2020). Exchange Bias in a La0.67Sr0.33MnO3/NiO Heterointerface Integrated on a Flexible Mica Substrate. *ACS Appl. Mat. Interfaces* 12 (35), 39920–39925. doi:10.1021/acsami.0c12935

Hwang, H. Y., Cheong, S. W., Ong, N. P., and Batlogg, B. (1996). Spin-polarized Intergrain Tunneling in La2/3Sr1/3MnO3. *Phys. Rev. Lett.* 77, 2041–2044. doi:10.1103/PhysRevLett.77.2041

Kang, B. S., Wang, H., MacManus-Driscoll, J. L., Li, Y., Jia, Q. X., Mihut, I., et al. (2006). Low Field Magnetotransport Properties of (La0.7Sr0.3MnO3)0.5: (ZnO)0.5 Nanocomposite Films. *Appl. Phys. Lett.* 88 (19), 192514. doi:10.1063/1.2197317

Kang, Y.-M., Kim, H.-J., and Yoo, S.-I. (2012). Enhanced Low-Field Magnetoresistance of La0.7Sr0.3Mn1+Do3-Mn3O4Composite Films Prepared by *Ex-Situ* Solid Phase Crystallization. *J. Magnetics* 17 (4), 265–270. doi:10.4283/jmag.2012.17.4.265

Liao, Z., and Zhang, J. (2019). Metal-to-insulator Transition in Ultrathin Manganite Heterostructures. *Appl. Sci.* 9 (1), 144. doi:10.3390/app9010144

Liu, J., Wang, X., Gao, X., Wang, H., Jian, J., Huang, J., et al. (2020). Multifunctional Self-Assembled BaTiO3-Au Nanocomposite Thin Films on Flexible Mica Substrates with Tunable Optical Properties. *Appl. Mater. Today* 21, 100856. doi:10.1016/j.apmt.2020.100856

Liu, W., and Wang, H. (2020). Flexible Oxide Epitaxial Thin Films for Wearable Electronics: Fabrication, Physical Properties, and Applications. *J. Materiomics* 6 (2), 385–396. doi:10.1016/j.jmat.2019.12.006

Liu, Y.-K., Yin, Y.-W., and Li, X.-G. (2013). Colossal Magnetoresistance in Manganites and Related Prototype Devices. *Chin. Phys. B* 22 (8), 087502. doi:10.1088/1674-1056/22/8/087502

Ma, C.-H., Chen, E.-L., Lai, Y.-H., Chen, Y.-C., Chang, L., and Chu, Y.-H. (2020). Flexible Transparent Heteroepitaxial Conducting Oxide with Mobility Exceeding 100 Cm2 V−1 S−1 at Room Temperature. *NPG Asia Mater* 12 (1), 70. doi:10.1038/s41427-020-00251-2

Millis, A. J., Darling, T., and Migliori, A. (1998). Quantifying Strain Dependence in "Colossal" Magnetoresistance Manganites. *J. Appl. Phys.* 83 (3), 1588–1591. doi:10.1063/1.367310

Moshnyaga, V., Damaschke, B., Shapoval, O., Belenchuk, A., Faupel, J., Lebedev, O. I., et al. (2003). Structural Phase Transition at the Percolation Threshold in Epitaxial (La0.7Ca0.3MnO3)1-X: (MgO)x Nanocomposite Films. *Nat. Mater* 2 (4), 247–252. doi:10.1038/nmat859

Navin, K., and Kurchania, R. (2018). Structural, Magnetic and Transport Properties of the La0.7Sr0.3MnO3-ZnO Nanocomposites. *J. Magnetism Magnetic Mater.* 448, 228–235. doi:10.1016/j.jmmm.2017.06.035

Ning, X., Wang, Z., and Zhang, Z. (2014). Large, Temperature-Tunable Low-Field Magnetoresistance in La0.7Sr0.3MnO3:NiO Nanocomposite Films Modulated by Microstructures. *Adv. Funct. Mat.* 24 (34), 5393–5401. doi:10.1002/adfm.201400735

Ning, X., Wang, Z., and Zhang, Z. (2015). Controllable Self-Assembled Microstructures of La0.7Ca0.3MnO3:NiO Nanocomposite Thin Films and Their Tunable Functional Properties. *Adv. Mat. Interfaces* 2 (15), 1500302. doi:10.1002/admi.201500302

Shen, X., Mo, D., li, C., Wu, D., and Li, A. (2012). Strain Effects on Magnetic Characteristics of Ultrathin La0.7Sr0.3MnO3in Epitaxial La0.7Sr0.3MnO3/BaTiO3superlattices. *J. Appl. Phys.* 112, 123919. doi:10.1063/1.4770485

Sun, X., Huang, J., Jian, J., Fan, M., Wang, H., Li, Q., et al. (2018). Three-dimensional Strain Engineering in Epitaxial Vertically Aligned Nanocomposite Thin Films with Tunable Magnetotransport Properties. *Mat. Horiz.* 5 (3), 536–544. doi:10.1039/c8mh00216a

Sun, X., Li, Q., Huang, J., Jian, J., Lu, P., Zhang, X., et al. (2019). Strain and Property Tuning of the 3D Framed Epitaxial Nanocomposite Thin Films via Interlayer Thickness Variation. *J. Appl. Phys.* 125 (8), 082530. doi:10.1063/1.5053705

Tiwari, A., Jin, C., Kumar, D., and Narayan, J. (2003). Rectifying Electrical Characteristics of La0.7Sr0.3MnO3/ZnO Heterostructure. *Appl. Phys. Lett.* 83 (9), 1773–1775. doi:10.1063/1.1605801

Tokura, Y., and Tomioka, Y. (1999). Colossal Magnetoresistive Manganites. *J. Magnetism Magnetic Mater.* 200 (1), 1–23. doi:10.1016/S0304-8853(99)00352-2

Valencia, S., Castaño, O., Fontcuberta, J., Martı´nez, B., and Balcells, L. (2003). Enhanced Low Field Magnetoresistive Response in (La2/3Sr1/3MnO3)x/(CeO2)1−x Composite Thick Films Prepared by Screen Printing. *J. Appl. Phys.* 94 (4), 2524–2528. doi:10.1063/1.1589174

Wang, H., Zhang, J., Jia, Q., Xu, F., Tan, W., Huo, D., et al. (2014). Three-dimensional Strain State and Spacer Thickness-dependent Properties of Epitaxial Pr0.7Sr0.3MnO3/La0.5Ca0.5MnO3/Pr0.7Sr0.3MnO3 Trilayer Structure. *J. Appl. Phys.* 115, 233911. doi:10.1063/1.4884995

Wang, H., Yang, W., Su, K., Huo, D., and Tan, W. (2015). Exchange-bias Field Induced by Surface Inhomogeneities in Ferromagnetic/charge-Ordered Bilayer Structure. *J. Alloys Compd.* 648, 966–970. doi:10.1016/j.jallcom.2015.07.086

Wang, H. O., Chu, Z., Su, K. P., Tan, W. S., and Huo, D. X. (2016). Colossal Magnetoresistance of Pr0.7Sr0.3MnO3 Layer Grown on Charge-Ordered La0.5Ca0.5MnO3 Manganite Layer. *J. Alloys Compd.* 689, 69–74. doi:10.1016/j.jallcom.2016.07.165

Wang, H., Tan, W., Su, K., Huang, S., Tan, W., Liu, H., et al. (2017). In-plane Magnetic Anisotropy of La 0.7 Ca 0.3 MnO 3 Film Grown on (0001) Sapphire. *Thin Solid Films* 621, 1–5. doi:10.1016/j.tsf.2016.11.026

Wang, H., Zhang, H., Wang, Y., Tan, W., and Huo, D. (2021). Spin Glass Feature and Exchange Bias Effect in Metallic Pt/antiferromagnetic LaMnO3 Heterostructure. *J. Phys. Condens. Matter* 33, 285802. doi:10.1088/1361-648X/ac0023

Wu, Y. J., Wang, Z. J., Ning, X. K., Wang, Q., Liu, W., and Zhang, Z. D. (2018). Room Temperature Magnetoresistance Properties in Self-Assembled Epitaxial La0.7Sr0.3MnO3:NiO Nanocomposite Thin Films. *Mater. Res. Lett.* 6 (9), 489–494. doi:10.1080/21663831.2018.1482838

Yao, X. Y., Yuan, G. L., Liu, J.-M., Yang, Y., and Liu, Z. G. (2003). The Magneto-Transport and Low-Field Magnetoresistance in Double-Layer Manganites La2−2xSr1+2xMn2O7 with Insulating Second Phase. *Mater. Lett.* 57 (21), 3199–3205. doi:10.1016/s0167-577x(03)00025-9

Yen, M., Lai, Y. H., Kuo, C. Y., Chen, C. T., Chang, C. F., and Chu, Y. H. (2020). Mechanical Modulation of Colossal Magnetoresistance in Flexible Epitaxial Perovskite Manganite. *Adv. Funct. Mat.* 30 (40), 2004597. doi:10.1002/adfm.202004597

Yin, L., Wang, C., Shen, Q., and Zhang, L. (2017). Orientation Dependence of Structural, Electrical and Magnetic Properties of La0.9Sr0.1MnO3 Thin Films. *J. Alloys Compd.* 695, 257–262. doi:10.1016/j.jallcom.2016.10.199

Zhang, W., Chen, A., Khatkhatay, F., Tsai, C.-F., Su, Q., Jiao, L., et al. (2013). Integration of Self-Assembled Vertically Aligned Nanocomposite (La0.7Sr0.3MnO3)1-X: (ZnO)x Thin Films on Silicon Substrates. *ACS Appl. Mat. Interfaces* 5 (10), 3995–3999. doi:10.1021/am400068h

Zhang, Y., Cao, Y., Hu, H., Wang, X., Li, P., Yang, Y., et al. (2019). Flexible metal-insulator transitions based on van der waals oxide heterostructures. *ACS Appl. Mat. Interfaces* 11 (8), 8284–8290. doi:10.1021/acsami.8b22664

Zhang, W., Cheng, S., Rouleau, C. M., Kelley, K. P., Keum, J., Stavitski, E., et al. (2020). Unusual Electrical Conductivity Driven by Localized Stoichiometry Modification at Vertical Epitaxial Interfaces. *Mat. Horiz.* 7 (12), 3217–3225. doi:10.1039/d0mh01324b

Zhang, H., Wang, Y., Wang, H., Huo, D., and Tan, W. (2022). Room-temperature Magnetoresistive and Magnetocaloric Effect in La1−xBaxMnO3 Compounds: Role of Griffiths Phase with Ferromagnetic Metal Cluster above Curie Temperature. *J. Appl. Phys.* 131, 043901. doi:10.1063/5.0078188

Zheng, C., Zhu, K., Cardoso de Freitas, S., Chang, J.-Y., Davies, J. E., Eames, P., et al. (2019). Magnetoresistive Sensor Development Roadmap (Non-recording Applications). *IEEE Trans. Magn.* 55 (4), 1–30. doi:10.1109/tmag.2019.2896036

Conflict of Interest: The authors declare that the research was conducted in the absence of any commercial or financial relationships that could be construed as a potential conflict of interest.

Publisher's Note: All claims expressed in this article are solely those of the authors and do not necessarily represent those of their affiliated organizations, or those of the publisher, the editors, and the reviewers. Any product that may be evaluated in this article, or claim that may be made by its manufacturer, is not guaranteed or endorsed by the publisher.